Frequency Optimization of a Loosely Coupled Underwater Wireless Power Transfer System Considering Eddy Current Loss

Zhengchao Yan, *Student Member, IEEE*, Yiming Zhang, *Member, IEEE*, Tianze Kan, *Student Member, IEEE*, Fei Lu, *Member, IEEE*, Kehan Zhang, Baowei Song, and Chunting Chris Mi, *Fellow, IEEE*

***Abstract*—Wireless power transfer (WPT) has attracted much attention in recent years. In an underwater WPT system, the eddy current loss tends to be non-negligible as the frequency or the coil current increases. Thus, it is crucial to analyze the eddy current loss in an underwater WPT system. The analytical model of the eddy current loss of a coreless WPT system in the seawater is established with Maxwell's equations. The expressions of the electric field intensity and the eddy current loss are derived. The eddy current loss is analyzed in different circumstances to illustrate the impacts of related factors. For a WPT system in the air, there is an optimum resonant frequency, for a higher frequency leads to a larger induced voltage, but will result in larger coil losses simultaneously. However, the optimum resonant frequency will be shifted because of the eddy current loss in the seawater. Then, the optimum operating frequency is obtained based on the analytical model. It is found that the optimum operating frequency is supposed to be larger than the resonant frequency to achieve the maximum dc–dc efficiency in the seawater. An underwater WPT prototype was built and the experimental results verified the theoretical analysis.**

***Index Terms*—Wireless power transfer (WPT), eddy current loss, resonant frequency, analytical model, underwater.**

I. Introduction

WIRELESS power transfer (WPT) technology has a number of advantages compared to the traditional power delivery due to its nonphysical connection between the power source and the load [1]–[4], which is suitable for battery charging of underwater electrical equipment [5]–[10] without a complex and costly sealing structure. Feezor *et al*. [8] developed a wireless charging system, which could transfer 200 W of power and signals for autonomous underwater vehicles (AUVs). Since then, McGinnis *et al*. [9] proposed a WPT system for AUVs to transfer 240-W power with 70% dc–dc efficiency. Li *et al*. [10] studied the effects of gaps between the transmitter and the receiver and designed a 400-W system with 90% efficiency across a 2-mm gap. Shi *et al*. [11] introduced a hull-compatible coaxial coil structure and evaluated the characteristics of the semiconductor loss, the copper loss, and the core loss using a circuit model and the finite element analysis. Orekan *et al*. [12] proposed a maximum power efficiency tracking method to estimate the real-time coupling coefficient in an underwater WPT system, which can effectively track the maximum efficiency of over 85%. Fang *et al*. [13] developed an underwater WPT system, containing two couplers and a closed cable, which can transfer power and data to the underwater sensors. He *et al*. [14] presented a three-dimensional omnidirectional underwater WPT system, the transmitter coil of which is made up of three mutually orthogonal loops. The simulation results showed the output power and the transmission efficiency can be improved greatly by adjusting the phase differences among the three loops compared to the conventional system.

In the seawater environment, the eddy current loss generated in the seawater must be taken into account, which will also affect the transmission efficiency of the WPT system. Cheng *et al*. [15] proposed an underwater WPT system based on a semi-closed core structure. The power loss was studied comparatively in the air, freshwater, and seawater. It is shown that the core loss and copper loss in these three media were essentially the same. The significant difference occurs in the eddy current loss. Itoh *et al*. [16] designed a WPT system for the swimming robot fish, which showed the eddy current loss had a sharp rise due to the increasing frequency. Yan *et al*. [17] proposed an arc electromagnetic coupler. The eddy current loss and the transmission efficiency are analyzed by the finite element method. Zhou *et al*. [18] proposed a single-turn model of a circular coil with a ferrite core to calculate the eddy current loss of the underwater WPT system. Then, the transmission efficiency is analyzed. However,

Manuscript received January 18, 2018; revised April 19, 2018 and May 22, 2018; accepted June 17, 2018. Date of publication July 9, 2018; date of current version December 28, 2018. This work was supported in part by the Natural Science Basic Research Program of Shaanxi Province under Grant 2018JM5033 and in part by the China Scholarship Council. *(Corresponding author: Chunting Chris Mi.)*

Z. Yan is with the School of Marine Science and Technology, Northwestern Polytechnical University, Xi'an 710072, China, and also with the Department of Electrical and Computer Engineering, San Diego State University, San Diego, CA 92182 USA (e-mail: yanzc1991@gmail.com).

Y. Zhang, T. Kan, F. Lu, and C. C. Mi are with the Department of Electrical and Computer Engineering, San Diego State University, San Diego, CA 92182 USA (e-mail: zhangym07@gmail.com; bigtreehust@gmail.com; feilu@umich.edu; mi@ieee.org).

K. Zhang and B. Song are with the School of Marine Science and Technology, Northwestern Polytechnical University, Xi'an 710072, China (e-mail: zhangkehan210@163.com; songbaowei@nwpu.edu.cn).

Color versions of one or more of the figures in this paper are available online at http://ieeexplore.ieee.org.

Digital Object Identifier 10.1109/TIE.2018.2851947

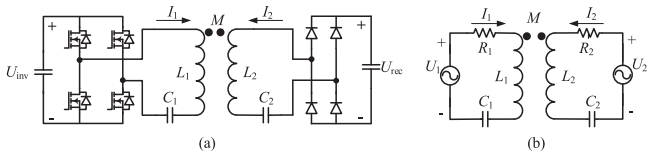

Fig. 1. SS WPT system. (a) Topology. (b) Equivalent circuit.

the ferrite is assumed to be infinite in the analytical model, which is not precise.

In this paper, a coreless WPT system is established, which has a lower weight than that with the ferrite. The model based on Maxwell's equations to calculate the eddy current loss in the seawater is proposed, which is more accurate. Finite element analysis is applied to verify the proposed calculation model. Both the resonant frequency and the operating frequency are optimized based on the analytical model. An underwater WPT prototype is set up to validate the analysis.

II. Wireless Charging System in the Air

The topology and the equivalent circuit of a wireless charging system with series–series (SS) compensation are shown in Fig. 1. The SS compensation topology is chosen because it has the advantage of constant current output, which can be easily controlled to charge the battery. In Fig. 1, U_{inv} and U_1 denote the dc and ac voltages of the inverter, respectively; L_1, C_1, and R_1 are the self-inductance, capacitance, and equivalent resistance of the transmitter; I_1 is the root-mean-square value of the transmitter current. U_{rec}, U_2, I_2, L_2, C_2, and R_2 are the counterparts on the receiver side. M is the mutual inductance between the transmitter and the receiver.

Neglecting the equivalent resistances of the transmitter and the receiver at the resonant state, the transmitter and the receiver currents are

$$I_1 = \frac{U_2}{\omega_0 M}. \tag{1}$$

$$I_2 = \frac{U_1}{\omega_0 M} \tag{2}$$

where ω_0 denotes the resonant angular frequency. Then, the output power can be expressed as

$$P_{\text{out}} = \omega_0 M I_1 I_2. \tag{3}$$

Assume that $R_1 = R_2$ and $L_1 = L_2$ in the system, the transmission efficiency η can be calculated as

$$\eta = \frac{P_{\text{out}}}{P_{\text{out}} + I_1^2 R_1 + I_2^2 R_2} = \frac{1}{1 + \frac{1}{kQ}\left(\frac{I_1}{I_2} + \frac{I_2}{I_1}\right)} \tag{4}$$

where k is the coupling coefficient, Q is the quality factor of the transmitter and the receiver, defined by

$$Q = \frac{\omega_0 L_1}{R_1} = \frac{\omega_0 L_2}{R_2}. \tag{5}$$

The transmission efficiency is maximized when $I_1 = I_2$, and the maximum transmission efficiency is

$$\eta_{\max} = \frac{1}{1 + \frac{2}{kQ}} = \frac{T_Q}{T_Q + 2} \tag{6}$$

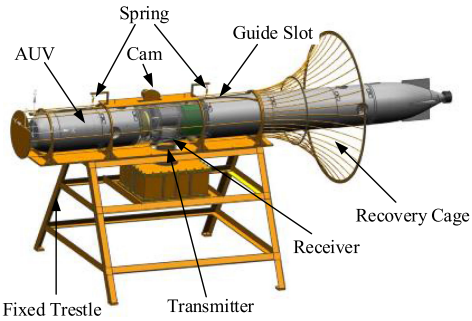

Fig. 2. General overview of the underwater WPT system.

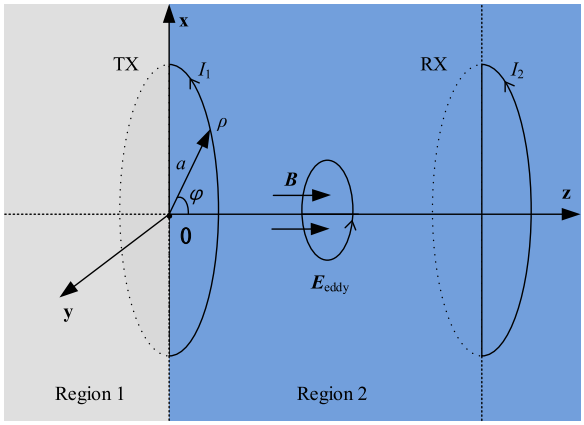

Fig. 3. Simplified calculation model of the electric field.

where T_Q is the figure of merit [19], defined by $T_Q = kQ$, and a higher T_Q results in a higher maximum transmission efficiency.

III. Eddy Current Loss in Seawater

In the application of a WPT system in the air, the power losses mainly lie in the core loss of the ferrite and the copper loss of the coils. However, when it comes to the application in the seawater environment, the eddy current loss generated in the seawater must be taken into account, which will also affect the transmission efficiency of the WPT system. Fig. 2 shows the general overview of an underwater WPT system. The secondary side and primary side are installed on the abdomen of the AUV and the base station, respectively. The system parameters can be kept relatively stable through this docking structure. To calculate the eddy current loss in the seawater, the electric field intensity should be calculated firstly.

A. Electric Field Intensity

Zhou *et al.* [18] proposed a single-turn model of a circular coil with a ferrite core to calculate the eddy current loss of the underwater WPT system. However, the ferrite is assumed to be infinite, which is not precise. This paper proposes a spiral planar coil without ferrite to theoretically calculate the eddy current loss in the seawater, which is more accurate. A single-turn transmitter coil is first studied in the cylindrical coordinate. Fig. 3 shows the simplified model of the electric field. The entire space is full of seawater. It is assumed that the coil is on

the imaginary inner boundary surface: $z = 0$, which means the boundary conditions on both sides of the surface are known. Then, the study area is divided into two regions by the inner boundary surface to calculate the electromagnetic field. Thus, there are no external excitation currents in the study area, which merely distribute on the inner boundary surface.

The surface current density on an arbitrary point $\boldsymbol{Q}(\rho,\varphi,0)$ of the inner boundary surface is

$$\boldsymbol{K}(\rho,\varphi,0) = I_1\delta(\rho-a)\,\boldsymbol{e}_\varphi \tag{7}$$

where ρ denotes the radius, a represents the radius of the coil, and $\boldsymbol{e}_\varphi$ is the circumferential unit vector.

Assume that the medium is linear, homogeneous and isotropic, then the electromagnetic field is expressed based on Maxwell's equations. For convenience, the dot on the complex vector is omitted

$$\nabla\times\boldsymbol{H} = \boldsymbol{J} + \frac{\partial \boldsymbol{D}}{\partial t} = \boldsymbol{J} + j\omega\boldsymbol{D}, \nabla\times\boldsymbol{E} = -\frac{\partial \boldsymbol{B}}{\partial t} = -j\omega\boldsymbol{B} \tag{8}$$

$$\nabla\cdot\boldsymbol{B} = 0, \nabla\cdot\boldsymbol{D} = 0 \tag{9}$$

$$\boldsymbol{B} = \mu\boldsymbol{H}, \boldsymbol{J} = \sigma\boldsymbol{E}, \boldsymbol{D} = \varepsilon\boldsymbol{E} \tag{10}$$

where $\boldsymbol{H}$ and $\boldsymbol{B}$ denote the magnetic field intensity and the magnetic flux density, respectively. $\boldsymbol{E}$ and $\boldsymbol{J}$ are the electric field intensity and the conduction current density, respectively. $\boldsymbol{D}$ is the electric displacement vector. Eliminating $\boldsymbol{H}$ gives the following constraint equation:

$$\begin{cases} \nabla^2\boldsymbol{E}_i + k_i^2\boldsymbol{E}_i = 0 \\ \nabla\cdot\boldsymbol{E}_i = 0 \\ i = 1,2 \end{cases}. \tag{11}$$

Due to the cylindrical symmetry, the electric field intensity $\boldsymbol{E}_i$ merely has the circumferential component, namely $\boldsymbol{E}_i = E_{i\varphi}\boldsymbol{e}_\varphi$. In the cylindrical coordinate system

$$\frac{\partial^2 E_{i\varphi}}{\partial\rho^2} + \frac{1}{\rho}\frac{\partial E_{i\varphi}}{\partial\rho} + \frac{\partial^2 E_{i\varphi}}{\partial z^2} + \left(k_i^2 - \frac{1}{\rho^2}\right)E_{i\varphi} = 0, i = 1,2 \tag{12}$$

where $\boldsymbol{E}_i$ denotes the electric field intensity in each area, and the space wave number is defined as $k^2 = -j\omega\mu(\sigma + j\omega\varepsilon)$, wherein, μ, σ, and ε denote the permeability, the electrical conductivity, and the permittivity of the medium, respectively. The boundary conditions and the infinity conditions are

$$\begin{cases} E_{2\varphi} - E_{1\varphi} = 0, z = 0 \\ \frac{1}{\mu_r}\frac{\partial E_{2\varphi}}{\partial z} - \frac{1}{\mu_r}\frac{\partial E_{1\varphi}}{\partial z} = j\omega\mu_0 I_1\delta(\rho-a), z = 0 \end{cases} \tag{13}$$

$$\begin{cases} \lim_{z\to-\infty} E_{1\varphi} = 0 \\ \lim_{z\to+\infty} E_{2\varphi} = 0 \end{cases} \tag{14}$$

where μ_r is the relative permeability and μ_0 is the permeability of the vacuum. Based on the separation of variables [20], the general solution of (12) can be expressed as

$$E_{i\varphi}(\rho,z) = \int_0^\infty J_1(\lambda\rho)\left(C_{1i}e^{u_i z} + C_{2i}e^{-u_i z}\right)d\lambda \tag{15}$$

where $\lambda\in(0,+\infty)$, an intermediate variable, will be eliminated in the later derivation; $u = \sqrt{\lambda^2 - k^2}$; C_{1i} and C_{2i} are the undetermined coefficients. $J_1(x)$ is the first-order Bessel function of the first species. By substituting (15) into (13) and (14), C_{1i} and C_{2i} can be determined. Then, the electric field intensity caused by the *ii*-turn can be obtained

$$\begin{cases} \boldsymbol{E}_{1\varphi t,ii} = -\frac{j\omega\mu I_1 a_{ii}}{2}\int_0^\infty \frac{\lambda}{u}\cdot J_1(\lambda a_{ii})J_1(\lambda\rho)\,e^{uz}d\lambda\boldsymbol{e}_\varphi, z<0 \\ \boldsymbol{E}_{2\varphi t,ii} = -\frac{j\omega\mu I_1 a_{ii}}{2}\int_0^\infty \frac{\lambda}{u}\cdot J_1(\lambda a_{ii})J_1(\lambda\rho)\,e^{-uz}d\lambda\boldsymbol{e}_\varphi, z>0 \end{cases}. \tag{16}$$

Assume that the turn numbers of the transmitter and the receiver are the same, namely $N_1 = N_2 = N$. The electric field intensity of an arbitrary point (ρ, z) in the study area $\boldsymbol{E}_{2t}$, which is caused by the *N*-turn transmitter coil, is obtained based on the principle of superposition

$$\boldsymbol{E}_{2t} = \sum_{ii=1}^{N}\boldsymbol{E}_{2\varphi t,ii}. \tag{17}$$

The same procedure can be easily adopted to obtain the electric field intensity caused by the receiver current, which can be expressed as

$$\begin{cases} \boldsymbol{E}_{1\varphi r,jj} = -\frac{j\omega\mu I_2 a_{jj}}{2}\int_0^\infty \frac{\lambda}{u}J_1(\lambda a_{jj})\,J_1(\lambda\rho)\,e^{-u(z-d)}d\lambda\mathbf{e}_\varphi, \\ \qquad\qquad\qquad\qquad\qquad\qquad z > d \\ \boldsymbol{E}_{2\varphi r,jj} = -\frac{j\omega\mu I_2 a_{jj}}{2}\int_0^\infty \frac{\lambda}{u}J_1(\lambda a_{jj})\,J_1(\lambda\rho)\,e^{u(z-d)}d\lambda\mathbf{e}_\varphi, \\ \qquad\qquad\qquad\qquad\qquad\qquad z < d \\ \boldsymbol{E}_{2r} = \sum_{jj=1}^{N}\boldsymbol{E}_{2\varphi r,jj} \end{cases} \tag{18}$$

where d is the gap between the transmitter and the receiver. $\boldsymbol{E}_{2r}$ is the electric field intensity of an arbitrary point (ρ, z) in the study area, which is caused by *N*-turn receiver coil.

B. Unilateral Eddy Current Loss

The permeability of the air and the seawater are almost the same, while there is a significant difference in the electrical conductivity. The alternating electromagnetic field, generated by the high-frequency alternating currents in the coils, will eventually give rise to the eddy current loss. In the underwater WPT systems, the eddy current loss should be all dimensional. However, the transmitter is in the base station and the receiver is in the vehicle, such as an AUV. The vicinity below the transmitter and above the receiver is indeed full of air. In the previous simulations and experiments, we made a comparison of placing the seawater between the transmitter and the receiver and putting the seawater all dimensional. The results show that the total losses of these two cases are almost the same, which indicates most of the eddy current loss exists in the space between the transmitter and the receiver in the practical applications. Therefore, this paper only considers the eddy current loss in the seawater between the transmitter and the receiver. The eddy current loss caused by the transmitter is calculated as (19), shown at the bottom of the next page. V is the study domain. h_sea and r_sea denote the seawater height and the seawater radius, respectively.

C. Bilateral Eddy Current Loss

In an underwater WPT system, the electric field $\boldsymbol{E}_2$ is the vector sum of the electric field $\boldsymbol{E}_{2t}$ and $\boldsymbol{E}_{2r}$ in the direction of $\boldsymbol{e}_\varphi$, caused by the transmitter current I_1 and the receiver current I_2, respectively. I_1 equals I_2 in the system. There is a phase difference θ between the transmitter current I_1 and the receiver current I_2, which is approximately the same as the phase difference of $\boldsymbol{E}_{2t}$ and $\boldsymbol{E}_{2r}$ [21]. Thus, the eddy current loss, which can be calculated as (20), shown at the bottom of this page, is generated by the synthesized electric field intensity $\boldsymbol{E}_2$.

IV. Frequency Optimization

The eddy current loss has a significant rise as the resonant frequency and coil currents increase [21]. Therefore, it is necessary to choose a lower resonant frequency or a smaller coil current for underwater WPT systems. While in some underwater applications, the coreless WPT system is preferred for its low weight and elimination of magnetic losses. Moreover, in order to make the system compact, the resonant frequency should be relatively high [22]. With the same coil currents, the higher frequency leads to a larger induced voltage, thus a larger output power and higher efficiency can be achieved. Therefore, there is an optimum frequency in the underwater WPT system.

A. Resonant Frequency

At the resonant state, the output power of a WPT system can be approximately calculated as

$$P_{\text{out}} = \omega_0 M I_1 I_2 = \omega_0 M I_2^2 \tag{21}$$

where $I_1 = I_2$ is settled in the system. The mutual inductance M is a constant value as the system setup is fixed. Based on the aforementioned derivation, the eddy current loss in the seawater can be expressed as

$$P_{\text{eddy}} = m\omega_0^2 I_2^2 \tag{22}$$

where m is a coefficient, relative to the permeability and the electrical conductivity of the seawater, the dimension of the seawater region, the radii of the transmitter and the receiver, and the gap between the transmitter and the receiver, which can be expressed as (23), shown at the bottom of this page.

When the system dimension is fixed, m is a constant. Then, the ratio of the eddy current loss and the output power can be obtained as

$$P_{\text{eddy}}/P_{\text{out}} = \frac{m\omega_0}{M}. \tag{24}$$

It can be seen that the ratio is proportional to the resonant frequency, and is independent of the coil currents. Therefore, for a constant power output, it is practical to decrease the resonant frequency to reduce the proportion that the eddy current loss occupies the output power. However, decreasing the coil currents makes no difference to this ratio. For a WPT system in the air, there is an optimum resonant frequency, a higher frequency leads to a larger induced voltage, but will result in larger coil losses simultaneously. However, the optimum resonant frequency will be shifted to a smaller value in the seawater than that in the air to restrain the ratio of the eddy current loss.

B. Operating Frequency

As shown in the previous section, the eddy current loss is generated by the synthesized electric field intensity $\boldsymbol{E}_2$, which is the vector sum of the electric field intensity $\boldsymbol{E}_{2t}$ and $\boldsymbol{E}_{2r}$ in the direction of $\boldsymbol{e}_\varphi$, caused by the transmitter and the receiver currents, respectively. Therefore, changing the phase difference θ between the transmitter current I_1 and the receiver current I_2 by frequency tuning to the optimum resonant point, will result in a variation of the phase difference between $\boldsymbol{E}_{2t}$ and $\boldsymbol{E}_{2r}$.

In Fig. 1(b), by applying Kirchhoff's law in the receiver side, we have

$$U_2 - R_2 I_2 = jX_2 I_2 + j\omega M I_1 \tag{25}$$

where ω denotes the operating angular frequency, X_2 is the reactance of the receiver, i.e.,

$$X_2 = \omega L_2 - \frac{1}{\omega C_2}. \tag{26}$$

$$P_{\text{eddy1}} = \int_V \sigma |\boldsymbol{E}_{2t}|^2 dV = \frac{\sigma\mu^2\omega^2 I_1^2}{4} \int_0^{2\pi} \int_0^{r\_\text{sea}} \int_0^{h\_\text{sea}} \left| \sum_{ii=1}^{N} \int_0^{\infty} \frac{\lambda}{u} \cdot a_{ii} J_1(\lambda a_{ii}) J_1(\lambda\rho) e^{-uz} d\lambda \right|^2 d\varphi d\rho dz \tag{19}$$

$$\begin{aligned} P_{\text{eddy}} = \int_V \sigma |\boldsymbol{E}_2|^2 dV = \int_V \sigma |\boldsymbol{E}_{2t} + \boldsymbol{E}_{2r}|^2 dV = \frac{\sigma\mu^2\omega^2 I_2^2}{4} \int_0^{2\pi} \int_0^{r\_\text{sea}} \int_0^{h\_\text{sea}} \left| \sum_{ii=1}^{N} \int_0^{\infty} \frac{\lambda}{u} \cdot a_{ii} J_1(\lambda a_{ii}) J_1(\lambda\rho) e^{-uz} d\lambda \right. \\ \left. + e^{j\theta} \sum_{jj=1}^{N} \int_0^{\infty} \frac{\lambda}{u} \cdot a_{jj} J_1(\lambda a_{jj}) J_1(\lambda\rho) e^{u(z-d)} d\lambda \right|^2 d\varphi d\rho dz \end{aligned} \tag{20}$$

$$m = \frac{\sigma\mu^2}{4} \int_0^{2\pi} \int_0^{r\_\text{sea}} \int_0^{h\_\text{sea}} \left| \sum_{ii=1}^{N} \int_0^{\infty} \frac{\lambda}{u} \cdot a_{ii} J_1(\lambda a_{ii}) J_1(\lambda\rho) e^{-uz} d\lambda + e^{j\theta} \sum_{jj=1}^{N} \int_0^{\infty} \frac{\lambda}{u} \cdot a_{jj} J_1(\lambda a_{jj}) J_1(\lambda\rho) e^{u(z-d)} d\lambda \right|^2 d\varphi d\rho dz. \tag{23}$$

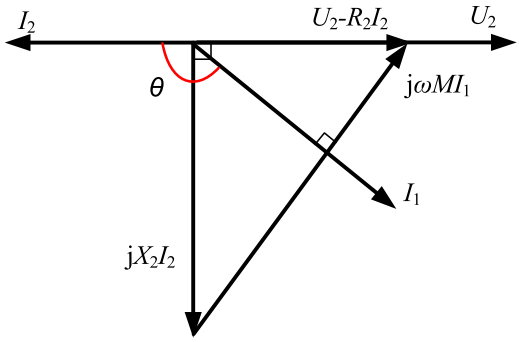

Fig. 4. Phasor diagram of the WPT system.

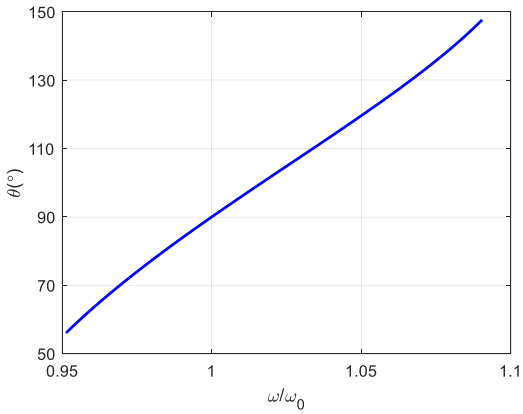

Fig. 5. Phase difference varying with normalized operating angular frequency.

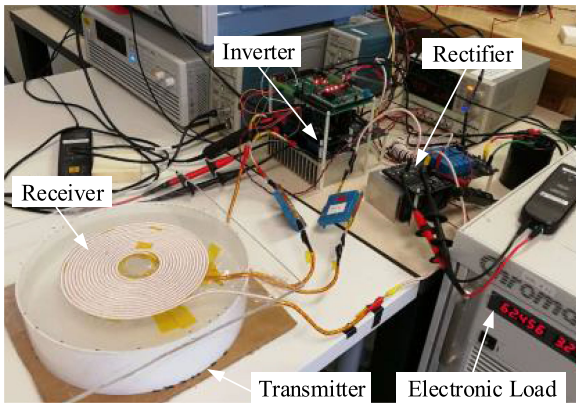

Fig. 6. Experimental prototype.

The resonant angular frequency ω_0 is

$$\omega_0 = \frac{1}{\sqrt{L_1 C_1}} = \frac{1}{\sqrt{L_2 C_2}}. \tag{27}$$

With frequency tuning in Fig. 1(b), if $\omega > \omega_0$, the phasor diagram of the ac currents and voltages is plotted in Fig. 4

In this paper, L_1 and L_2 are designed to be the same and I_1 and I_2 are adjusted to be identical. The phase difference θ can be calculated as

$$\cos(\pi - \theta) = \frac{X_2 I_2}{\omega M I_1} = \frac{\omega L_2 - \frac{1}{\omega C_2}}{\omega k L_2} = \frac{1}{k}\left(1 - \frac{\omega_0^2}{\omega^2}\right). \tag{28}$$

Thus

$$\theta = \arccos\left[\frac{1}{k}\left(\frac{\omega_0^2}{\omega^2} - 1\right)\right]. \tag{29}$$

As for $\omega < \omega_0$, the same equation can be obtained.

As shown in Fig. 5, the phase difference between I_1 and I_2 is approximately proportional to the normalized operating angular frequency, which means the phase difference between $\boldsymbol{E}_{2t}$ and $\boldsymbol{E}_{2r}$ increases as the operating frequency rises around the resonant frequency. Based on the Cosine Theorem, the synthesized electric field intensity $\boldsymbol{E}_2$ decreases, thus the eddy current loss will decrease. Therefore, the optimum operating frequency is supposed to be larger than the resonant frequency to restrain the eddy current loss in the seawater.

TABLE I
SYSTEM SPECIFICATIONS AND CIRCUIT PARAMETERS

Note	symbol	Value
Transmitter inductance	L_1	27.4 μH
Receiver inductance	L_2	26.8 μH
Mutual inductance	M	5.1 μH
Coupling coefficient	k	0.19
Number of turns	N_1, N_2	16
gap	d	66 mm
Coil dimension		Φ176 mm × 4 mm
Seawater region		Φ260 mm × (22 mm-88 mm)
Resonant frequency	f_0	60 kHz-600 kHz

V. Calculations, Simulations, and Experiments

In order to verify the aforementioned theoretical analysis, an underwater experimental prototype is implemented, as shown in Fig. 6. The system specifications and the circuit parameter values are tabulated in Table I. Planar spiral coils are adopted as the transmitter and the receiver with a turn number of 16, which are composed of tightly wound AWG 38 Litz wires with 3.9-mm diameter. The inverter input voltage and current, the battery voltage and current, the dc–dc efficiency, the input power, and the output power are all measured by YOKOGAWA Power Analyzer WT1800. The seawater is placed in a bucket, of which the diameter is larger than the coil diameter. The gap between the transmitter and the bottom surface of the seawater is 7 mm and the gap between the receiver and the top surface of the seawater is 14 mm. The resonant frequency ranges from 60 to 600 kHz by changing the matching capacitances.

A. Analysis of Eddy Current Loss

The eddy current loss caused by the transmitter current in the seawater is firstly studied. The experiments are carried out.

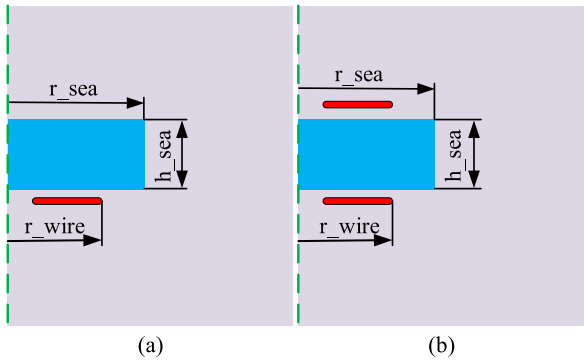

Fig. 7. Simulation model. (a) Only transmitter. (b) Transmitter and receiver.

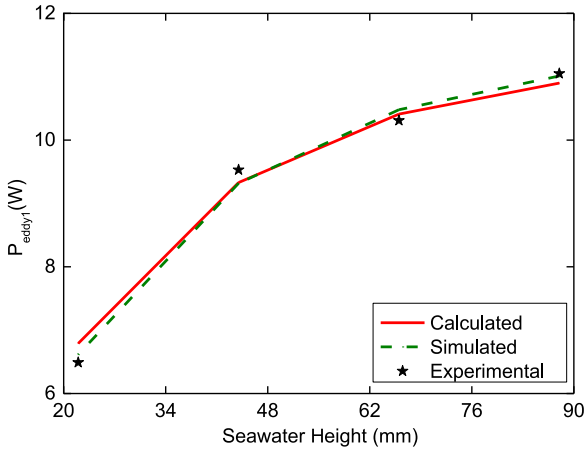

Fig. 8. Eddy current loss with seawater height.

The corresponding simulations in Comsol Multiphysics are also conducted as displayed in Fig. 7(a). Two-dimensional axisymmetric simulation model is adopted due to the circular dimension of the transmitter and the receiver. The transmitter currents are kept the same under the cases with and without the seawater. Therefore, the eddy current loss in the seawater will be the difference of the total losses of the two cases, namely, $P_{\mathrm{eddy1}} = P_{\mathrm{loss\_seawater}} - P_{\mathrm{loss\_air}}$.

When the transmitter current is 5 A and the resonant frequency is 504.5 kHz, the calculated, simulated, and experimental eddy current losses with different seawater heights are shown in Fig. 8. The experimental and the simulated results agree well with the calculations. Furthermore, the eddy current loss has a moderate ascent with an increasing seawater height. The eddy current loss is 10.3 W when the seawater height is 66 mm.

Then, the eddy current loss generated by the transmitter and receiver currents is investigated with a seawater height of 44 mm. Simultaneously, the gap between the transmitter and the receiver is fixed at 66 mm, which is large enough for the underwater equipment. The experiments are carried out and the corresponding simulations in Comsol Multiphysics are established as displayed in Fig. 7(b). Fig. 9 shows the magnitude of the electric field of the study domain caused by the transmitter and the

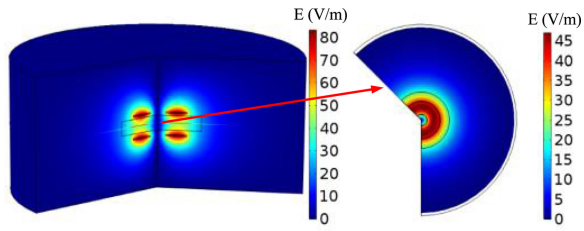

Fig. 9. Electric field distribution.

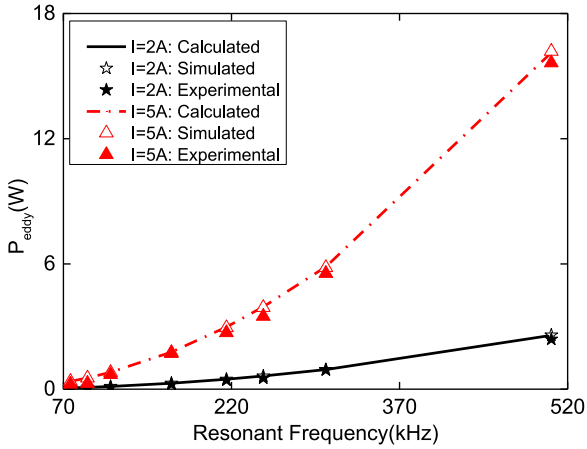

Fig. 10. Eddy current loss caused by the transmitter and the receiver.

receiver current. The arrow points to the electric field distribution on the intermediate cross-section of the seawater region, which is parallel to the transmitter and the receiver. It is shown that the electric field only has the circumferential component and is much stronger in the vicinity of the coils.

The transmitter current and the receiver current, which are identical, are kept the same under the cases with and without the seawater. Therefore, the eddy current loss will be also indirectly measured by the difference of the total losses of the two cases, namely, $P_{\mathrm{eddy}} = P_{\mathrm{loss\_seawater}} - P_{\mathrm{loss\_air}}$. Fig. 10 shows the calculated, simulated, and experimental results caused by the combined effect of the transmitter and the receiver varying with resonant frequencies when $I_1 = I_2 = 2$ A and $I_1 = I_2 = 5$ A. It indicates that the eddy current loss rises as the resonant frequency or the coil current increases. When the resonant frequency is higher than 100 kHz, the eddy current loss increases sharply with the increasing resonant frequencies. The experimental results well match the simulated and calculated results.

B. Frequency Optimization

The ratio of the eddy current loss and the output power varying with the resonant frequency and the coil current are shown in Fig. 11. It can be seen that the ratio between the eddy current loss and the output power is proportional to the resonant frequency and is independent of the coil current, which verifies the theoretical analysis. Thus, we can decrease the resonant frequency other than the coil current to decrease this ratio.

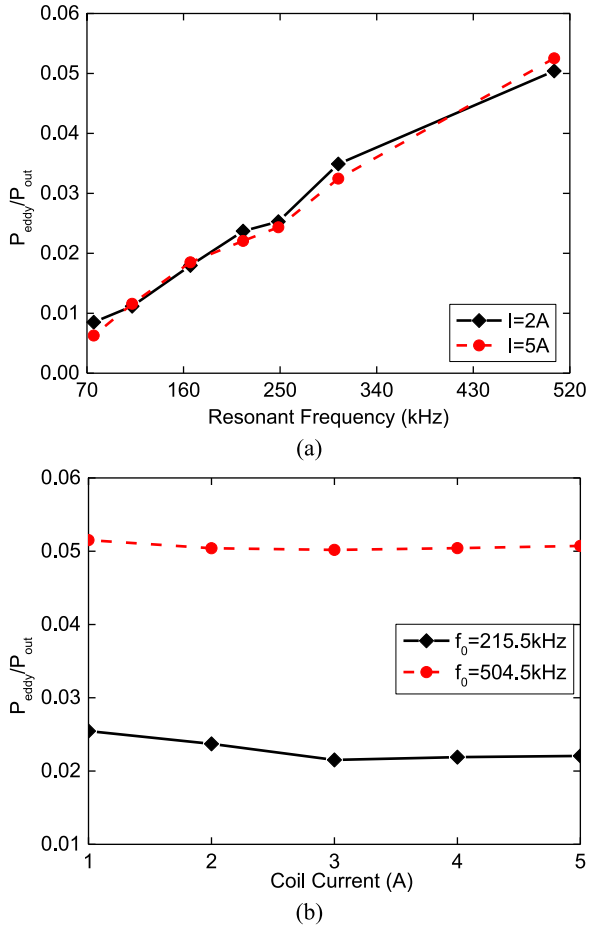

Fig. 11. Ratio of the eddy current loss and the output power. (a) With resonant frequency. (b) With coil current.

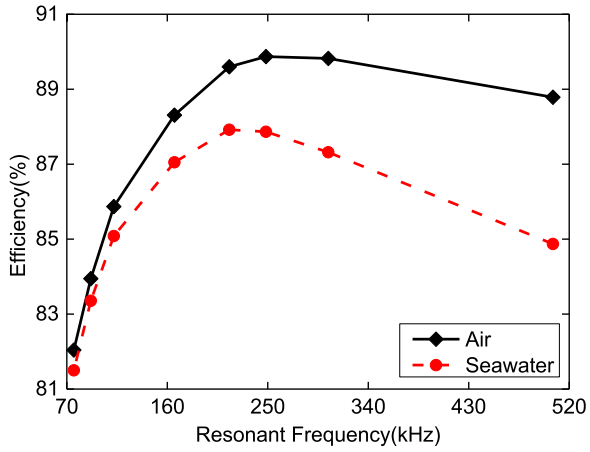

Fig. 12. System efficiency varying with the resonant frequency.

In practical applications, it is necessary to satisfy the power requirement. By regulating the output power to be 200 W and $I_1 = I_2$, the dc–dc efficiency varying with the resonant frequency is plotted in Fig. 12. It indicates that the system efficiency peaks at a certain resonant frequency in the air and the seawater, respectively. The optimum resonant frequency in the seawater is 215.5 kHz, smaller than that in the air of 248.4 kHz due to the eddy current loss in the seawater.

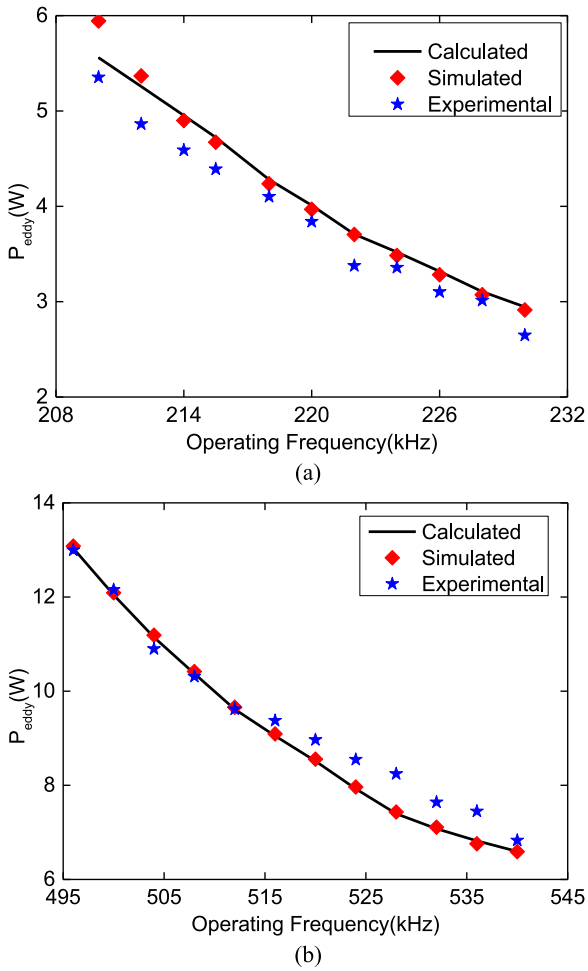

Fig. 13. Eddy current loss with operating frequency. (a) $f_0 = 215.5$ kHz. (b) $f_0 = 504.5$ kHz.

With frequency tuning, the output power is fixed at 200 W and two cases are studied. Case 1: $f_0 = 215.5$ kHz; Case 2: $f_0 = 504.5$ kHz. The eddy current losses of these two cases varying with the operating frequency are shown in Fig. 13. It is interesting that the eddy current loss significantly decreases with the increasing operating frequency in both cases. It is because the phase difference between I_1 and I_2 becomes larger with the increasing operating frequency. It demonstrates the theoretical analysis in Section IV.

Fig. 14 shows the system efficiency with the increasing operating frequency in both cases. It can be seen that the system efficiency in the air peaks when the operating frequency equals the resonant frequency. While in the seawater, the optimum operating frequency should be larger than the resonant frequency to achieve the maximum dc–dc efficiency. This is because the electric fields caused by I_1 and I_2 counteract with each other versus an increasing operating frequency at the vicinity of the resonant frequency, leading to a decreased eddy current loss, as analyzed in Section IV-B. The phenomenon is not that significant because of the limited seawater region between the

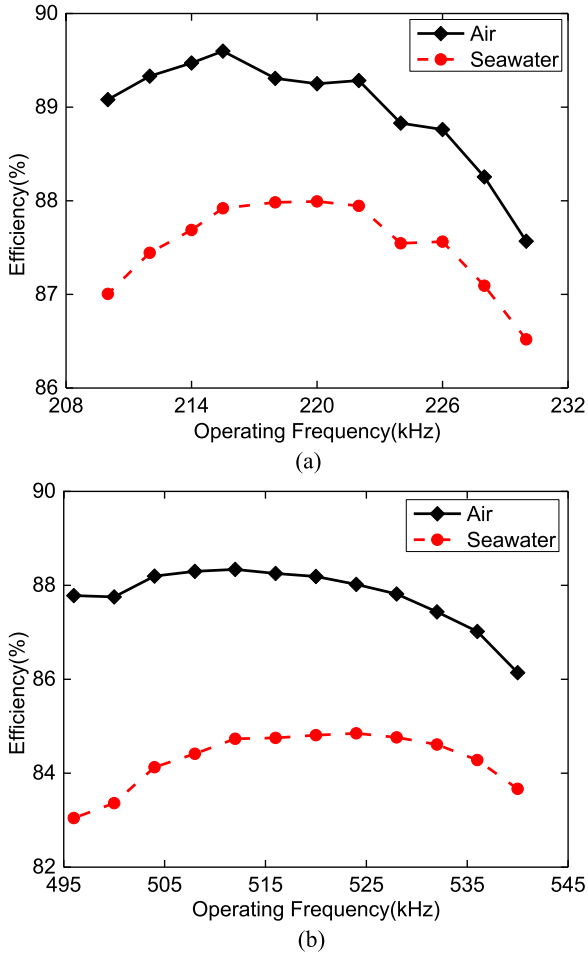

Fig. 14. System efficiency with operating frequency. (a) $f_0 =$ 215.5 kHz. (b) $f_0 =$ 504.5 kHz.

transmitter and the receiver, however, it is capable of understanding the characteristics of the underwater WPT systems.

VI. Conclusion

In this paper, the eddy current loss of a coreless underwater WPT system was modeled and analyzed. The expressions of the electric field intensity and the eddy current loss were derived under arbitrary frequencies. The eddy current loss was analyzed for different gaps, frequencies, and transmitter currents. Based on the eddy current loss model, the resonant frequency and operating frequency were optimized. An underwater WPT prototype was built and the experimental results verified the theoretical analysis.

It was found that the eddy current loss in the seawater has a sharp increase with the increasing resonant frequency, because of which the optimum resonant frequency in the seawater is shifted to a smaller value than that in the air. Moreover, the optimum operating frequency of a WPT system in the seawater should be larger than the resonant frequency to achieve the maximum dc–dc efficiency, different from the fact that the optimal operating frequency of a WPT system in the air should equal the resonant frequency of the receiver.

Due to the limitation of the experimental condition, the phenomenon is not so obvious because of a relatively small eddy current loss in the experiment. Nevertheless, this paper helps to better understand and optimize the design of the underwater WPT systems.

References

[1] C. C. Mi, G. Buja, S. Y. Choi, and C. T. Rim, "Modern advances in wireless power transfer systems for roadway powered electric vehicles," *IEEE Trans. Ind. Electron.*, vol. 63, no. 10, pp. 6533–6545, Oct. 2016.

[2] Y. Zhang, T. Lu, Z. Zhao, F. He, K. Chen, and L. Yuan, "Employing load coils for multiple loads of resonant wireless power transfer," *IEEE Trans. Power Electron.*, vol. 30, no. 11, pp. 6174–6181, Nov. 2015.

[3] J. P. K. Sampath, A. Alphones, and D. M. Vilathgamuwa, "Optimization of wireless power transfer system with a repeater against load variations," *IEEE Trans. Ind. Electron.*, vol. 64, no. 10, pp. 7800–7809, Oct. 2017.

[4] S. Li and C. C. Mi, "Wireless power transfer for electric vehicle applications," *IEEE J. Emerg. Sel. Topics Power Electron.*, vol. 3, no. 1, pp. 4–17, Mar. 2015.

[5] A. P. Hu and S. Hussmann, "Improved power flow control for contactless moving sensor applications," *IEEE Power Electron. Lett.*, vol. 2, no. 4, pp. 135–138, Dec. 2004.

[6] T. Kan, R. Mai, P. P. Mercier, and C. Mi, "Design and analysis of a three-phase wireless charging system for lightweight autonomous underwater vehicles," *IEEE Trans. Power Electron.*, vol. 33, no. 8, pp. 6622–6632, Aug. 2018.

[7] T. Kojiya, F. Sato, H. Matsuki, and T. Sato, "Automatic power supply system to underwater vehicles utilizing non-contacting technology," in *Proc. OCEANS'04. MTTS/IEEE TECHNO-OCEAN'04*, 2004, pp. 2341–2345.

[8] M. D. Feezor, F. Y. Sorrell, and P. R. Blankinship, "An interface system for autonomous undersea vehicles," *IEEE J. Ocean. Eng.*, vol. 26, no. 4, pp. 522–525, Oct. 2001.

[9] T. McGinnis, C. P. Henze, and K. Conroy, "Inductive power system for autonomous underwater vehicles," in *Proc. OCEANS 2007*, 2007, pp. 1–5.

[10] Z. Li, D. Li, L. Lin, and Y. Chen, "Design considerations for electromagnetic couplers in contactless power transmission systems for deep-sea applications," *J. Zhejiang Univ.—Sci. C*, vol. 11, pp. 824–834, 2010.

[11] J. Shi, D. Li, and C. Yang, "Design and analysis of an underwater inductive coupling power transfer system for autonomous underwater vehicle docking applications," *J. Zhejiang Univ.—Sci. C*, vol. 15, pp. 51–62, 2014.

[12] T. Orekan, P. Zhang, and C. Shih, "Analysis, design and maximum power efficiency tracking for undersea wireless power transfer," *IEEE J. Emerg. Sel. Topics Power Electron.*, vol. 6, no. 2, pp. 843–854, Oct. 2017.

[13] C. Fang, X. Li, Z. Xie, J. Xu, and L. Xiao, "Design and optimization of an inductively coupled power transfer system for the underwater sensors of ocean buoys," *Energies*, vol. 10, 2017, Art. no. 84.

[14] Z. He, Y. Wang, L. Ding, and X. Nie, "Research on three-dimensional omnidirectional wireless power transfer system for subsea operation," in *Proc. OCEANS 2017-Aberdeen*, 2017, pp. 1–5.

[15] Z. Cheng, Y. Lei, K. Song, and C. Zhu, "Design and loss analysis of loosely coupled transformer for an underwater high-power inductive power transfer system," *IEEE Trans. Magnet.*, vol. 51, no. 7, pp. 1–10, Jul. 2015.

[16] R. Itoh, Y. Sawahara, T. Ishizaki, and I. Awai, "Wireless power transfer to moving ornamental robot fish in aquarium," in *Proc. IEEE 3rd Global Conf. Consumer Electron.*, 2014, pp. 459–460.

[17] Z. Yan, K. Zhang, H. Wen, and B. Song, "Research on characteristics of contactless power transmission device for autonomous underwater vehicle," in *Proc. OCEANS 2016-Shanghai*, 2016, pp. 1–5.

[18] J. Zhou, D. Li, and Y. Chen, "Frequency selection of an inductive contactless power transmission system for ocean observing," *Ocean Eng.*, vol. 60, pp. 175–185, 2013.

[19] Y. Zhang, K. Chen, F. He, Z. Zhao, T. Lu, and L. Yuan, "Closed-form oriented modeling and analysis of wireless power transfer system with constant-voltage source and load," *IEEE Trans. Power Electron.*, vol. 31, no. 5, pp. 3472–3481, May 2016.

[20] D. A. Hill *et al.*, *Time-Harmonic Electromagnetic Fields*. New York, NY, USA: Wiley, 1961.

[21] K. Zhang, Z. Zhu, B. Song, and D. Xu, "A power distribution model of magnetic resonance WPT system in seawater," in *Proc. IEEE Annu. Southern Power Electron. Conf.*, 2016, pp. 1–4.

[22] F. Lu, H. Zhang, H. Hofmann, and C. Mi, "A high efficiency 3.3 kW loosely-coupled wireless power transfer system without magnetic material," in *Proc. IEEE Energy Convers. Congr. Expo.*, 2015, pp. 2282–2286.

Zhengchao Yan (S'18) received the B.S. degree in mechanical design, manufacturing, and automation from Northwestern Polytechnical University, Xi'an, China, in 2013, where he is currently working toward the Ph.D. degree in electrical engineering.

In 2017, he received funding from the China Scholarship Council and became a joint Ph.D. student with the Department of Electrical and Computer Engineering, San Diego State University, San Diego, CA, USA. His research interests focus on wireless power transfer, including electromagnetic field calculation, coil design, and compensation topologies.

Yiming Zhang (S'13–M'16) received the B.S. and Ph.D. degrees in electrical engineering from Tsinghua University, Beijing, China, in 2011 and 2016, respectively.

He is currently a Postdoctoral Researcher with San Diego State University, San Diego, CA, USA. His research interests include wireless power transfer for electric vehicles and mobile phones, and resonant converters.

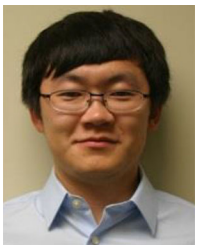

Tianze Kan (S'15) received the B.Eng. degree in electrical engineering and automation from Huazhong University of Science and Technology, Wuhan, China, in 2011, and the M.S. degree in electrical engineering from the University of Southern California, Los Angeles, CA, USA, in 2013. He is currently working toward the Ph.D. degree in electrical and computer engineering in the joint doctoral program between San Diego State University, San Diego, CA, USA, and the University of California San Diego, La Jolla, CA.

His research interests include power electronics and inductive-based wireless power transfer, especially on coil design and compensation topologies.

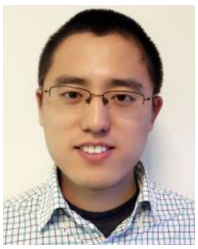

Fei Lu (S'12–M'17) received the B.S. and M.S. degrees from Harbin Institute of Technology, Harbin, China, in 2010 and 2012, respectively, and the Ph.D. degree from the University of Michigan, Ann Arbor, Michigan, USA, in 2017, all in electrical engineering.

He is currently a Postdoc Researcher with San Diego State University, San Diego, CA, USA. His research topic focuses on the application of electric vehicle charging.

Kehan Zhang was born in Shaanxi, China, in 1971. He received the Ph.D. degree from Xi'an Jiaotong University, Xi'an, China, in 2000.

He is currently an Associate Professor and Master Instructor with Northwestern Polytechnical University. His research interests focus on DSP-based brushless dc motor control system and wireless power transfer.

Baowei Song received the B.S. degree in mechanical engineering from Northwestern Polytechnical University, Xi'an, China, in 1986 and the Ph.D. degree in mechatronic engineering from Northwestern Polytechnical University in 1999.

He is currently a Professor and the Vice-President of Northwestern Polytechnical University. His research interests include general technical research of underwater vehicles.

Chunting Chris Mi (S'00–A'01–M'01–SM'03–F'12) received the B.S.E.E. and M.S.E.E. degrees in electrical engineering from Northwestern Polytechnical University, Xi'an, China, in 1985 and 1988, respectively. He received the Ph.D. degree in electrical engineering from the University of Toronto, Toronto, Ontario, Canada, in 2001.

He is a Professor and Chair of Electrical and Computer Engineering and the Director of the Department of Energy funded Graduate Automotive Technology Education Center for Electric Drive Transportation, San Diego State University (SDSU), San Diego, CA, USA. Prior to joining SDSU, he was with with the University of Michigan, Dearborn, MI, USA, from 2001 to 2015. His research interests include electric drives, power electronics, electric machines, renewable-energy systems, and electric and hybrid vehicles.